https://doi.org/10.5194/os-2020-114
Preprint. Discussion started: 16 December 2020

Ocean Science
Discussions
Open Access
EGU

Laboratory experiments on the influence of stratification and a bottom sill on seiche damping

Karim Medjdoub[1], Imre M. Jánosi[1], and Miklós Vincze[1,2]

[1]von Kármán Laboratory of Environmental Flows; Eötvös Loránd University, Pázmány P. sétány 1/A, Budapest H-1117, Hungary
[2]MTA-ELTE Theoretical Physics Research Group, Pázmány P. sétány 1/A, Budapest H-1117, Hungary

Correspondence: Miklós Vincze (mvincze@general.elte.hu)

Abstract. The damping of water surface standing waves (seiche modes) and the associated excitation of baroclinic internal waves are studied experimentally in a quasi-two-layer laboratory setting with a topographic obstacle at the bottom, representing a seabed sill. We find that topography-induced baroclinic wave drag indeed contributes markedly to seiche damping in such systems. Two major pathways of barotropic-baroclinic energy conversions were observed: the stronger one – involving short-wavelength internal modes of large amplitudes – may occur when the node of the surface seiche is situated above the close vicinity of the sill. The weaker, less significant other pathway is the excitation of long waves, internal seiches along the pycnocline that may resonate with the low frequency components of the decaying surface forcing.

1 Introduction

Energy conversion over bathymetric formations is a key component of the global ocean dynamics and mixing (Wunsch and Ferrari, 2004). The coupling between barotropic tidal waves at the sea surface and internal gravity waves in the bulk facilitates heat and material exchange between the uppermost and deeper layers (Garrett, 2003; Lelong and Kunze, 2013; Morozov, 2018; Vic et al., 2019; Rippeth and Green, 2020; Stanev and Ricker, 2020). This largely interconnected dynamics is particularly pertinent in semi-enclosed basins, bays, and fjords with density profiles characterized by sharp gradients (Rattray Jr., 1960; Niiler, 1968; Bell Jr., 1975; Stigebrandt, 1980; Stigebrandt and Aure, 1989; Chapman and Giese, 1990; Münnich, 1996; Parsmar and Stigebrandt, 1997; Stigebrandt, 1999; Antenucci and Imberger, 2001, 2003; Inall et al., 2004; Cushman-Roisin et al., 2005; Johnsson et al., 2007; Boegman and Ivey, 2012; Park et al., 2016; Staalstrøm and Røed, 2016; Castillo et al., 2017; Roget et al., 2017; Stanev and Ricker, 2020; Xue et al., 2020).

The exchange between waves at the surface and at the pycnocline can be especially well studied in the situation where standing waves develop at the water surface, known as seiches (Chapman and Giese, 2001; de Carvalho Bueno et al., 2020). Such oscillatory motions of a water body are typically initiated by temporally changing wind stress, especially pulse-like wind bursts, or storms. Strong wind shear gets balanced by a certain tilt of the water surface throughout the basin, but when the storm subsides, the restoring forces, predominantly gravity, yield a damped "sloshing" of the free surface, until it settles in its equilibrium (horizontal) position. Tidal barotropic waves, even tsunamis and other seismic disturbances are known to generate large inflows into coastal harbors and may also yield strong seiche activity (Chapman and Giese, 2001).

https://doi.org/10.5194/os-2020-114
Preprint. Discussion started: 16 December 2020

The energy dissipation rate (or decay rate) of surface seiches in natural enclosed lakes, seas, fjords is determined by the physical properties of the fluid body (e.g. its stratification profile) and the geometry of the basin. In the presence of bottom topography, surface gravity waves generate internal waves, a process also referred to as barotropic to baroclinic energy conversion, or – in the specific case of tidal surface waves – tidal conversion. The first demonstration of such a wave excitation mechanism over a tilted bottom topography dates back to the work of Rattray Jr. (1960) in the case of a two-layer stratification. Niiler (1968) explained the observed current oscillation at the Florida Straits with the interaction of barotropic tides and the continental slope that yields a generation of baroclinic tidal waves, periodically modulating the flow. Although these pioneering studies did not consider the dissipative effect of the excited baroclinic modes on the surface waves, it is obvious that freely propagating internal waves use up a significant fraction of the energy stored in the surface oscillations, and hence speed up the decay of the latter.

Parsmar and Stigebrandt (1997) investigated the damping of tidally excited surface seiches in the Gullmar fjord of Sweden, whose bottom topography inolves a sill reaching up to the pycnocline between the saline seawater and the upper freshwater layer. They concluded that the drag caused by baroclinic internal wave excitation at the sill contributes far more to the damping of the seiche than bottom friction or other phenomena. They did not investigate, however, the effect of damping on the frequencies of the seiche modes, even though it is well known that damped oscillations typically exhibit decreased frequencies relative to the undamped systems. This aspect was addressed by the paper of Cushman-Roisin et al. (2005) who concluded that in enclosed water bodies (e.g. lakes) the oscillation periods of seiche modes do not depend on the stratification significantly, only up to the order of $\Delta\rho/\rho$, where $\Delta\rho$ denotes the density difference between the two layers, and ρ represents the characteristic (e.g. average) fluid density in the system. However, in semi-enclosed systems, such as bays, where freely propagating internal waves can "radiate" away, into the open ocean, the surface seiche period was found to be more sensitive to the stratification. This effect of internal wave excitation on the decay of surface seiches was further investigated by Wynne et al. (2019).

When the characteristic (e.g. diurnal) frequency of the wind forcing matches that of a seiche eigenmode, a resonant amplification of the latter may occur. However, as the seasonal changes of the freshwater inflow (e.g. from glacier runoff) influence the depth of the pycnocline, the natural frequencies of the internal waves also change, and – as the resonant frequencies shift – so does the decay coefficient of the dominant surface seiche mode, as shown by Antenucci and Imberger (2001, 2003).

Internal wave excitation by surface seiche modes has been investigated in laboratory experiments by Boegman and Ivey (2012) who modeled resonant barotropic-baroclinic energy conversion of a periodically forced shallow water system in a rectangular tank without topographic obstacles in order to quantify the energy flux pathways between the applied forcing and the internal wave field. A similar setting (i.e. a rectangular tank with a flat bottom) has also been studied recently by Xue et al. (2020), with a special focus on internal wave excitation and seiche damping.

Here we report on laboratory experiments in a narrow water tank, filled up with quasi two-layer salinity stratified water, with a vertical obstacle installed in the middle of the domain in the bottom layer. We analyze the damping of various surface and internal wave modes that develop after pulse-like initial seiche excitation at the water surface. To the best of our knowledge, these are the first experiments in the literature on surface seiche damping in the presence of a bottom sill yielding considerable baroclinic wave drag.

https://doi.org/10.5194/os-2020-114
Preprint. Discussion started: 16 December 2020

Ocean Science
Discussions
Open Access
EGU

The paper is organized as follows. Section 2 describes the experimental set-up and the applied data acquisition methods. In Section 3 we present our results on the relationship between surface seiche damping and the physical and geometrical properties of the experimental settings. Finally, we briefly discuss and summarize our findings in Section 4.

2 Set-up and methods

Our experiments were conducted in a transparent rectangular acrylic (Plexiglas) tank of length $L = 80$ cm and width $w = 5$ cm, filled up with quasi-two-layer stratified water, as shown in Fig.1a. The bottom layer of thickness $H_2 = 4$ cm consisted of saline water colored with blue food dye, whereas the upper layer of thickness H_1 was freshwater of the same temperature, colored red. To inhibit mixing at the interface (i.e. diapycnal mixing) during the filling-up procedure the freshwater of the upper layer was entering the surface slowly, through a sponge.

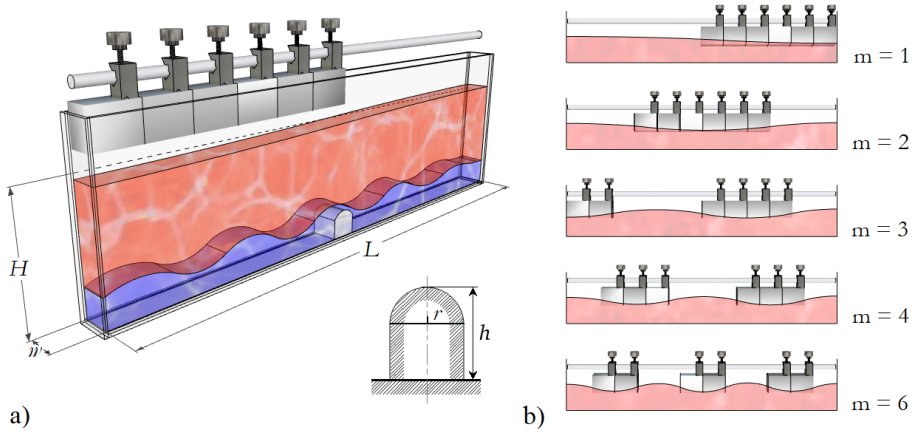

Figure 1. (a) The schematics of the set-up. The geometrical parameters of the tank are $L = 80$ cm, $w = 5$ cm, and $H_2 = h = 4$ cm. The shape of the obstacle is sketched in the bottom right corner ($h = 4$ cm, $r = 1.75$ cm). (b) The configurations of the six rubber foam bumpers of the wave maker for the excitation of the various surface seiche modes and the sketch of the corresponding waveform.

With each prepared stratification profile two configurations were studied. One with an upside-down U-shaped small plastic obstacle (Fig.1a) that was placed in the middle of the tank to the bottom. The obstacle's height h matched the thickness of the bottom (saline) layer: $h = H_2 = 4$ cm. In the other series of experiments the obstacle was removed from the tank (slowly, in the vertical direction, to minimize turbulent mixing) and the dynamics was studied in the absance of the topographic obstacle.

Each experiment series consisted of five runs with and five runs without the obstacle. A run was initiated as follows. A suspended wave maker consisting of a metallic rod and six rectangular rubber foam "bumpers" (Fig.1b) was placed above the water surface. The bumpers could be placed in various configurations along the rod to facilitate the excitation of surface seiche (standing wave) modes, as sketched in Fig.1b. The $m = 5$ pattern – where m denotes the number of nodes of the standing

https://doi.org/10.5194/os-2020-114
Preprint. Discussion started: 16 December 2020

Ocean Science
Discussions
Open Access
EGU

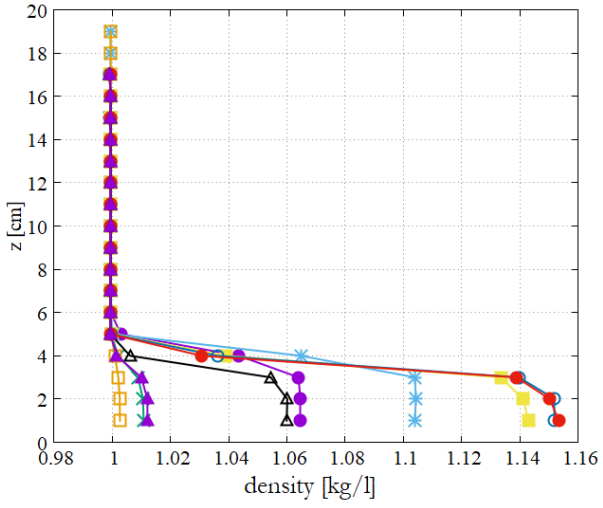

Figure 2. Density ρ as a function of vertical position z from the bottom, for all experiments series (cf. Table 1).

Table 1. Geometrical and physical characteristics of the experiment series.

Experiment series	#1	#2	#3	#4	#5	#6	#7	#8	#9
H_1 (cm)	11	11	15	15	13	13	13	13	13
ρ_2 (cm)	1.0592	1.0076	1.0872	1.0019	1.1114	1.1136	1.1114	1.0437	1.0084

waveform – was found to be very hard to excite with this device, therefore our analysis was restricted to experiments with surface seiche modes $m = 1, 2, 3, 4$, and 6. In the beginning of a run the suspended rod was pushed down to the water surface, reaching down to a depth of ca. 1 cm in a standardized manner and was then instantaneously pulled up, out of the water.

The prepared density profiles of the experiment series are presented in Fig.2, as measured by a conductivity probe, and the relevant adjustable parameters of the stratification, i.e. saline layer density ρ_2 and top layer thickness H_1 are summarized in Table 1 for all nine experiment settings.

The damping of the initiated surface sloshing and the internal dynamics was recorded by a an HD camera (at frame rate 30 fps and frame size 1080 px $\times$ 1920 px) facing the long sidewall of the tank perpendicularly, close to the middle of the tank. Afterwards, the open source correlation based feature tracking software Tracker (https://physlets.org/tracker/) was used to acquire the time series of surface and pycnocline motion.

https://doi.org/10.5194/os-2020-114
Preprint. Discussion started: 16 December 2020

3 Results

3.1 Qualitative description

The flow dynamics in the set-up is driven by the decaying surface waves initiated by a standardized instantaneous push of the wave maker. In the qualitative sense, the decay of the resulting surface standing waves is not affected by the presence or absence of the bottom obstacle (although the actual values of the decay rates are significantly different in the two configurations as will be discussed later). However, the dynamics in the bulk can be vastly different in the two cases: if the obstacle is installed, velocity shear can develop between the bottom and top layers that yields the excitation of baroclinic (internal) wave modes along the pycnocline. Whereas in the control runs – i.e. without obstacle – the vertical displacement of the surface and the pycnocline is found to be co-aligned at each time instant, as if in a homogeneous fluid (barotropic wave modes).

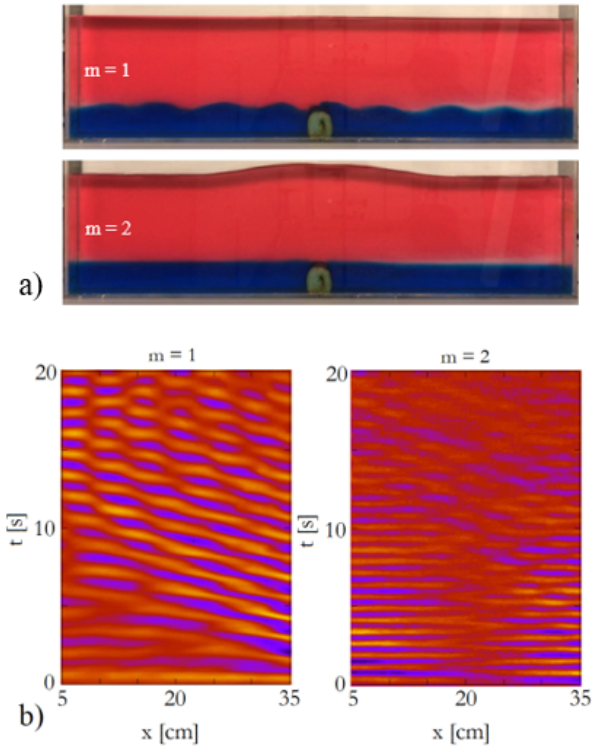

Figure 3. (a) Snapshots from experiments with $m = 1$ (top) and $m = 2$ (bottom) surface seiche modes (configuration #3, cf. Table 1). (b) Space-time plots of the same two experiments, showing the vertical dispacement of the pycnocline $\chi(x, t)$ in the left side of the tank (obstacle location is at $x = 40$ cm). The coloring in both panels is normalized with respect to the largest and smallest displacement values in the given space–time plot.

https://doi.org/10.5194/os-2020-114
Preprint. Discussion started: 16 December 2020

Yet, even if the obstacle is present, large amplitude internal waves do not necessarily get excited, as demonstrated in Fig.3. Panel a) shows snapshots from two experiments, characterized by the leading mode of the surface seiche that is $m = 1$ (base mode) and $m = 2$ in the top and bottom images, respectively. One can notice that in the former case, where a node of the surface wave form is located at the center of the tank, indicating purely horizontal flow right above the obstacle, slowly propagating internal waves of short wavelength appear "radiating away" from the obstacle with fairly large amplitudes. In the latter experiment, however, where the surface displacement has an antinode – and hence vertical oscillation of the fluid parcels – at the obstacle location, no progressive internal waves are visible.

The corresponding space-time plots of the pycnocline's displacement $\chi(x,t)$ relative to its initial unperturbed vertical position (i.e. $z = H_2$) are presented in Fig.3b, where the left panel shows the $m = 1$ and the right one the $m = 2$ case. (The horizontal range covers the region left of the obstacle, the coloring is normalized with respect to the largest negative and the largest positive values of χ from violet to orange in both panels.) After the initiation of the surface seiche (at $t = 0$) the slow leftward propagation of baroclinic waves dominates the picture in the $m = 1$ run; later the waves get reflected at the sidewall and thus evolve into internal standing wave-like interference patterns. In the $m = 2$ case the large-scale barotropic oscillation characterizes the entire domain with hardly any noticeable slowly propagating structures. This duality of internal wave excitation is apparent throughout the higher seiche modes as well: antisymmetric surface wave forms associated with odd values of m (see Fig.1b) tend to excite larger baroclinic wave activity via the obstacle placed in the geometrical center than the symmetric waves (even values of m).

3.2 Surface waves

Vertical displacement time series of the water surface $\eta(x,t)$ and the pycnocline $\chi(x,t)$ were logged at the vicinity of the sidewall (i.e. at $x \approx 0$ or L) in each experiment to ensure that all standing wave modes have antinode – i.e. maximum amplitude – at the measurement location. Such exemplary records are shown in the panels of the uppermost two rows of Fig.4 for the η and χ signals (red and blue curves, respectively) for modes $m = 1, 2,$ and 4.

The surface time series acquired at location $x = 0$ can be approximated as a sum of decaying sinusoidal oscillations in the following form:

$$\eta(0,t) \approx \sum_{i=1}^{N} A_i \exp(-C_i t) \sin(\omega_i t + \varphi_i), \tag{1}$$

where ω_i, φ_i and A_i denote the frequency, phase shift and initial amplitude of the i-th component, respectively, whereas $C_i(\omega_i)$ is the decay coefficient of the given mode. The fits have shown that the approximation of keeping only the two largest terms of the sum (i.e. setting $N = 2$) was sufficient to describe over 90% of the observed total variability in all runs and in many cases even the single-mode fit ($N = 1$) was enough to reach the same precision, thanks to the clear "quasi-monochromatic" initial conditions.

The Fourier amplitude spectra $A_\eta(f)$ and $A_\chi(f)$ of the $\eta(t)$ and $\chi(t)$ signals are presented in the third row of Fig.4 with a color coding identical to the corresponding time series themselves. The frequencies of the largest spectral peaks of $A_\eta(f)$ from each experiment were found to be in good agreement with the linear dispersion relation of homogeneous (non-stratified)

https://doi.org/10.5194/os-2020-114
Preprint. Discussion started: 16 December 2020

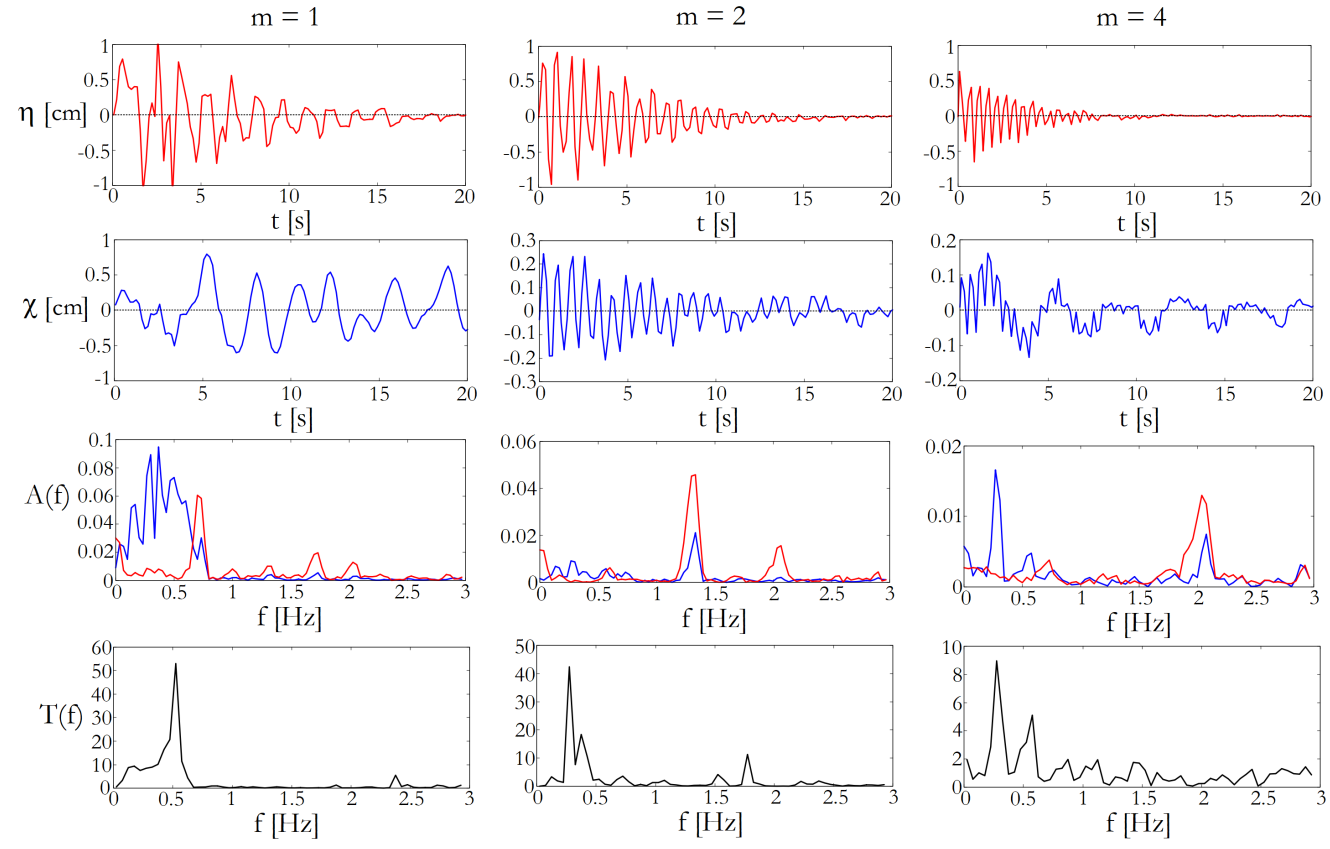

Figure 4. Time series and spectra from three exemplary runs (configuration #1, cf. Table 1) of dominant modes $m = 1$, $m = 2$, and $m = 4$ from the left. The panels of the top row shows the water surface displacement as a function of time t from the initiation, as tracked in the close vicinity of the sidewall. The displacement of the pycnocline χ at the sidewall is presented in the second row (note, that here, unlike in the $\eta(t)$ plots, the vertical range is different in all three panels). The Fourier spectra of the $\eta(t)$ (red) and $\chi(t)$ (blue) records are visible in the third row, whereas the bottom panels show the transfer function $T(f) = A_\chi(f)/A_\eta(f)$, i.e. the ratio of the spectra of the corresponding two spectra above.

surface gravity waves, which reads as

$$\omega = \sqrt{gk\tan(kH)}, \tag{2}$$

where H is the total water depth, g is the gravitational acceleration, and the wave number k is to be taken at $k(m) = \pi m/L$ for the dominant standing wave mode excited in the given run (cf. Fig.1). The match is demonstrated in Fig.5. In terms of the $\omega(m)$ relation, no systematic bias was found from this simple (linear, undamped) theoretical formula regardless of whether the experiment included the obstacle or not, or even whether the water was stratified or homogeneous. This is somewhat

https://doi.org/10.5194/os-2020-114
Preprint. Discussion started: 16 December 2020

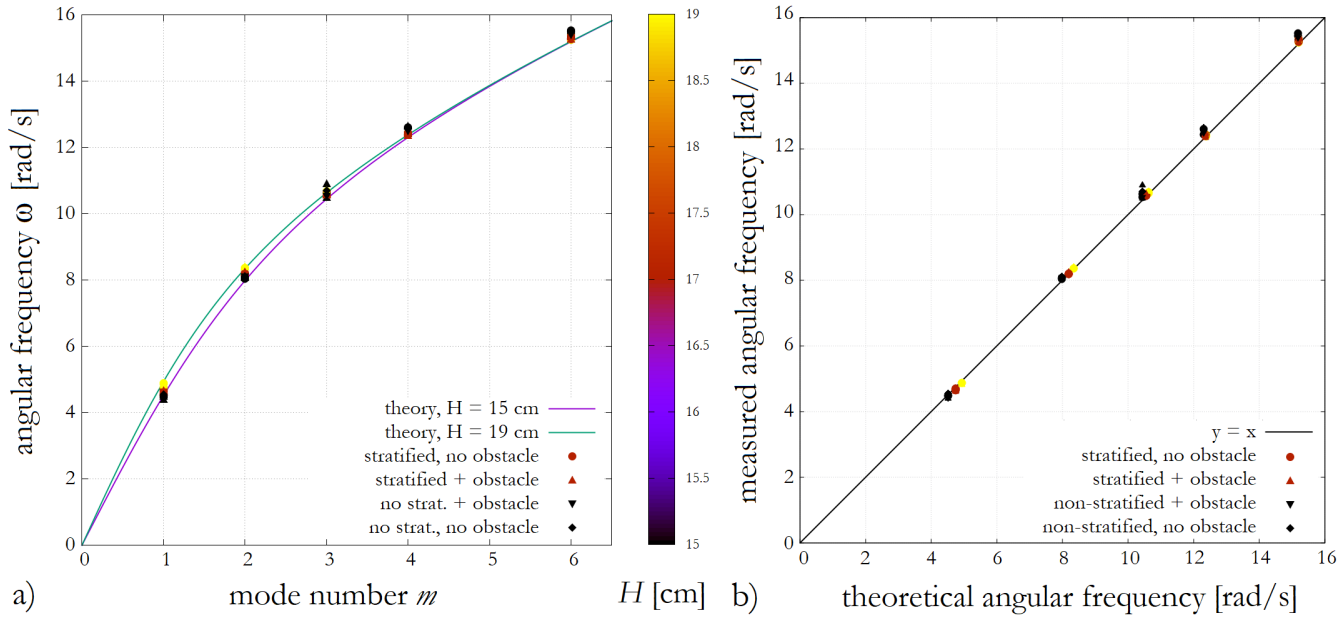

Figure 5. (a) The dispersion relation of water surface waves (2) expressed as a function of mode index m. The solid curves represent the the theoretical relationship for the shallowest ($H = 15$ cm) and deepest ($H = 19$ cm) configurations, and the data points indicate the measured values of angular frequency ω. The coloring is based on the total water height H. (b) Contrasting the calculated angular frequency ω from (2) to its measured value. The various experiment configurations are indicated by the shapes of the symbols in both panels (see legend).

surprising, since these factors are expected to influence the damping rate, and in a simple damped harmonic oscillator the exponential decay rate C and the characteristic frequency's shift relative to the undamped case are closely connected.

3.3 Source-filter dynamics

The surface waves exhibit faster damping than their internal counterparts and the dominant frequency components of the two may also largely differ. It is clearly visible from Fig.4 that the "internal" $\chi(t)$ signals possess more pronounced low-frequency variability than the $\eta(t)$ oscillations, even in the $m = 2$ and 4 modes, where the classic, topography-induced baroclinic wave generation is practically inhibited – due to the lack of significant velocity shear at the obstacle – as discussed earlier.

To understand this mechanism it is important to note that even if the surface seiche was a perfectly "monochromatic", single-frequency source signal, its exponential decay would still unavoidably introduce nonzero amplitudes into the low-frequency range of its spectrum (see, e.g. French (1971)), making it suitable for the excitation of slow internal oscillations. The resulting signal at the pycnocline can thus be understood as the outcome of a resonance-like amplification of certain characteristic frequency bands of the surface source signal.

The transfer function $T(f)$ of this frequency "filtering" can be defined as $T(f) = A_\chi(f)/A_\eta(f)$. Such empirical transfer functions for the experiments of Fig.4 are shown in the bottom row of subplots. In all cases, the maxima of $T(f)$ appear well

https://doi.org/10.5194/os-2020-114
Preprint. Discussion started: 16 December 2020

below the fundamental frequencies $f_i = \omega_i/(2\pi)$ of the source signal (1), consistently with the rule of thumb that interfacial internal propagation is typically around $\sqrt{\Delta\rho/\rho_0}$ times slower than that of surface waves.

The question arises of what kind of process determines the observed low-frequency amplification bands of $T(f)$. Combining the transfer functions of all five experiment runs (corresponding to different dominant m values) in a given stratification setting, one can define a cumulative transfer function by assigning the largest value of $T(f)$ obtained throughout all five runs to each frequency f, as represented by the gray shaded area of the combined spectrum in Fig.6a.

In the approximation of two homogeneous layers, separated by a sharp jump-wise pycnocline the dispersion relation of small amplitude interfacial internal waves (Massel, 2015) takes the form

$$\omega(k) = \sqrt{\frac{gk\Delta\rho}{\rho_1 \coth(H_1 k) + \rho_2 \coth(H_2 k)}}, \tag{3}$$

where k marks the wavenumber (in this case, along the pycnocline), H_1 and H_2 are the thicknesses and ρ_1 and ρ_2 are the densities of the top and bottom fluid layers, respectively (cf. Table 1), and $\Delta\rho = \rho_2 - \rho_1$ is their difference. This dispersion relation enables us to transform the $T(f)$ functions to the wavenumber domain, as shown in Fig.6b for four selected stratification settings. Here the frequency $f = \omega/(2\pi)$ is given on the horizontal axis and the wavenumber on the vertical one is expressed in the nondimensional units of $L/\lambda = Lk/(2\pi)$, with λ being the internal wavelength and L the length of the tank. The curves therefore represent the inverse of the dispersion relation (3), and their color scale marks the corresponding normalized cumulative transfer function $\overline{T}(f)$ (the normalization was carried out by setting the maximum of the $T(f)$ function as unity for each stratification).

Reorganizing the cumulative transfer functions this way, one can notice that the amplification peaks (high values of $\overline{T}$, colored yellow) tend to appear in the close vicinity of integer values of the nondimensional wave number, e.g. at $L/\lambda = 1; 2; 3; 5$ and 8, as marked by dotted horizontal lines in Fig.6b. These low frequency resonance peaks are thus seem to be related to standing wave generation at the pycnocline – internal seiche modes – whose wavelengths can fit integer times into the tank. Despite having much lower oscillation frequencies than the main peak of the "source" signal, these modes can still get excited due to the fact that the damping of the surface seiche introduces considerable amplitudes in the low-frequency spectral domain with which the internal standing waves can resonate.

3.4 Topographic energy conversion

The damping of surface waves in a stratified system is caused by the combination of factors such as the friction with the basin boundaries, diapycnal mixing, and barotropic-to-baroclinic energy conversion due to topographic effects. To separate the contribution of the latter we conducted control experiments with each studied stratification profile in which the obstacle was removed from the tank. We then compared the observed decay rates with the ones acquired with the obstacle in place.

The scatter plot in Fig.7a contrasts the the decay coefficient of the dominant surface seiche mode C_o – from fitting formula (1) – in each experiment with obstacle (hence the index o), with the corresponding no-obstacle value C_{no}. It is clearly visible that almost all data points spread in the $C_o > C_{\mathrm{no}}$ domain, but no systematic relationship could be found with the density ratio of the two layers (indicated by the coloring), or total water height H (marked by the different symbol shapes, see legend).

https://doi.org/10.5194/os-2020-114
Preprint. Discussion started: 16 December 2020

Ocean Science
Discussions
Open Access
EGU

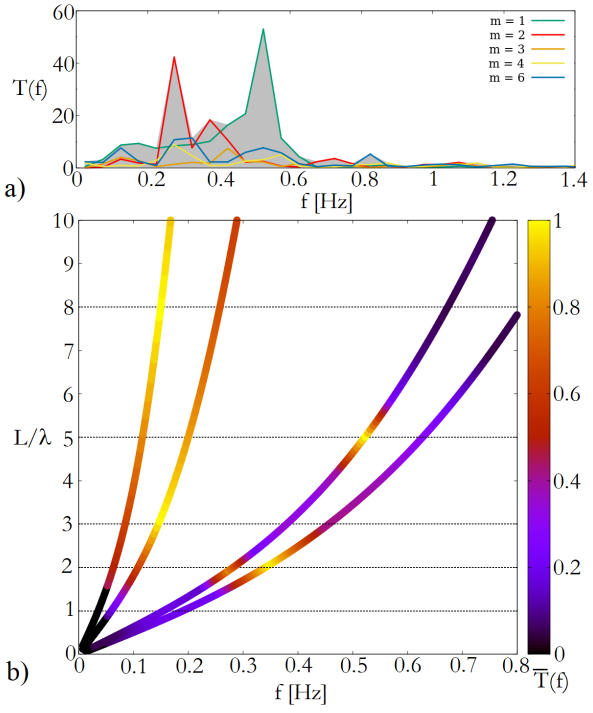

Figure 6. (a) The transfer functions $T(f)$ of all dominant excitation modes m in experiment series $\#1$, and their cumulative transfer function (grey shaded area). (b) The internal wave (inverse) dispersion relations as a function of frequency f based on (6) for four exemplary stratification settings (representing series $\#1$, $\#2$, $\#3$, and $\#4$). The coloring marks the normalized cumulative transfer functions $\overline{T}(f)$ as acquired from the corresponding experiment series.

There is, however, a significant difference between the two configurations in terms of the m-dependence of the decay coefficients, as shown in Fig.7b, where the C_o/C_{no} ratios are plotted for each experiment pair as a function of mode index m. Apparently, the relative increase of barotropic energy dissipation (damping) compared to the no-obstacle setting is the largest – up to a factor of 2.1 – at the odd wavenumbers $m = 1$ and 3 (note that the $m = 5$ mode could not be excited due to technical reasons, as mentioned earlier). This is in concert with the qualitative description provided in subsection 3.1, where we demonstrated that large amplitude internal waves having the same frequency as the surface wave are excited when the obstacle is situated below a surface seiche node.

4 Conclusions

In this experimental study, we analyzed the coupling between surface seiche modes and internal wave dynamics in a quasi-two-layer stratified system, and the effect of a topographic obstacle on the damping of the surface seiche. The decaying surface

https://doi.org/10.5194/os-2020-114
Preprint. Discussion started: 16 December 2020

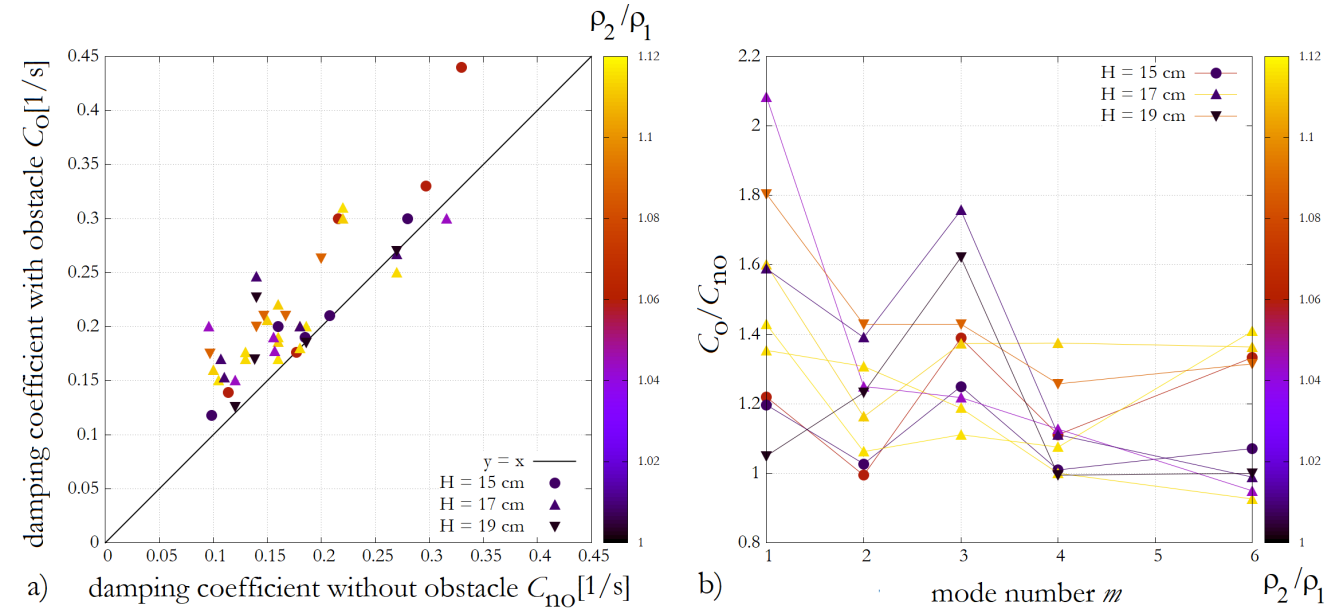

Figure 7. (a) Comparison of dominant mode surface seiche decay coefficients in paired experiments without (horizontal axis) and with (vertical axis) bottom obstacle. The solid line represents $y = x$. (b) The ratio of the damping coefficients C_o/C_{no} of paired experiments with and without obstacle as a function of dominant surface seiche mode index m. Symbol shapes and coloring mark the total water depth and the density ratio of the two layers, respectively, in both panels (see legend).

oscillations were initiated by a wave maker in a pulse-like manner, and the adjustable shape of this device enabled us to excite surface standing waves of rarely observable larger wavenumbers.

Two pathways of barotropic-to-baroclinic conversion were uncovered. Firstly, the "direct" excitation of short-wavelength propagating internal waves via the horizontal velocity shear emerging in the vicinity of the obstacle. These waves were easily noticeable along the pycnocline due to their relatively large amplitudes. Their periods matched the dominant sloshing timescale associated with the damping surface seiche. It is to be noted, that the most pronounced wave excitation, and thus the most prominent increase in the damping coefficient of the surface seiche was detected in the situations where the surface (standing) waveform was such that a node of the surface displacement was located above the bottom obstacle, that – in the geometry investigated here – means seiches of odd wavenumber indices.

Secondly, we found evidence for the excitation of slow, long wavelength internal seiching modes, whose half wavelength can fit roughly integer times onto the pycnocline between one sidewall and the obstacle (i.e. onto the half of the total basin length). The occurrence of such internal oscillations in this system is interesting as they have much lower characteristic frequencies than the surface seiche, i.e. the source signal. It appears, indeed, that a nontrivial source-filter dynamics can describe this phenomenon: the spectral structure of the decaying source signal includes low-frequency components that can resonate

https://doi.org/10.5194/os-2020-114
Preprint. Discussion started: 16 December 2020

with certain internal standing wave modes whose wavelengths are such that they fulfil the geometrical boundary conditions, representing a "band-pass filtering".

Comparing the dominant seiche decay rates with those from control runs without bottom topography, we demonstrated that in almost all cases internal wave activity yields a detectable increase of the damping, also for even seiche mode indices, where the "short wave" excitation is inhibited, as discussed above. In these cases internal wave dynamics can be attributed to the aforementioned slow wave (internal seiche) excitation pathway, but even this lesser effect appeared to be enough to yield significantly larger damping than the flat-bottom control runs.

Future research is planned to address the source-filter feedback effects in the system to better understand the relationship between the decay rates of the waves at the surface and the ones along the pycnocline. and to explore the dynamics of a more realistic, three-dimensional configuration, possibly involving the effect of Earth's rotation.

Author contributions. K.M. developed the set-up and performed the experiments. M.V. and K.M. conducted the evaluation of the data. All authors have contributed to the interpretation of results and the writing of the manuscript.

Competing interests. The authors declare that they have no conflict of interest.

Acknowledgements. We are thankful for the fruitful discussions with T. Tél. This paper was supported by the National Research, Development and Innovation Office (NKFIH) under Grant FK125024. The work of K. M. is supported by the Stipendium Hungaricum Scholarship of the Tempus Public Foundation. This paper is also supported the ÚNKP-18-4 New National Excellence Program (M.V.) of the Ministry of Human Capacities of Hungary.

https://doi.org/10.5194/os-2020-114
Preprint. Discussion started: 16 December 2020

References

Antenucci, J. P. and Imberger, J.: Energetics of long internal gravity waves in large lakes, Limnol. Oceanogr., 46, 1760–1773, https://doi.org/https://doi.org/10.4319/lo.2001.46.7.1760, 2001.

Antenucci, J. P. and Imberger, J.: The seasonal evolution of wind/internal wave resonance in Lake Kinneret, Limnol. Oceanogr., 48, 2055–2061, https://doi.org/https://doi.org/10.4319/lo.2003.48.5.2055, 2003.

Bell Jr., T. H.: Topographically generated internal waves in the open ocean, J. Geophys. Res. (1896-1977), 80, 320–327, https://doi.org/https://doi.org/10.1029/JC080i003p00320, 1975.

Boegman, L. and Ivey, G. N.: The dynamics of internal wave resonance in periodically forced narrow basins, J. Geophys. Res.: Oceans, 117, https://doi.org/https://doi.org/10.1029/2012JC008134, 2012.

Castillo, M. I., Pizarro, O., Ramírez, N., and Cáceres, M.: Seiche excitation in a highly stratified fjord of southern Chile: the Reloncaví fjord, Ocean Sci., 13, 145–160, https://doi.org/https://doi.org/10.5194/os-13-145-2017, https://os.copernicus.org/articles/13/145/2017/, 2017.

Chapman, D. and Giese, G.: Seiches, in: Encyclopedia of Ocean Sciences (2nd Edition), edited by Steele, J. H., pp. 5:344–350, Academic Press, Oxford, https://doi.org/https://doi.org/10.1016/B978-012374473-9.00128-4, 2001.

Chapman, D. C. and Giese, G. S.: A model for the generation of coastal seiches by deep-sea internal waves, J. Phys. Oceanogr., 20, 1459–1467, https://doi.org/https://doi.org/10.1175/1520-0485(1990)020<1459:AMFTGO>2.0.CO;2, 1990.

Cushman-Roisin, B., Willmott, A. J., and Biggs, N. R.: Influence of stratification on decaying surface seiche modes, Cont. Shelf Res., 25, 227–242, https://doi.org/https://doi.org/10.1016/j.csr.2004.09.008, 2005.

de Carvalho Bueno, R., Bleninger, T., Yao, H., and Rusak, J. A.: An empirical parametrization of internal seiche amplitude including secondary effects, Env. Fluid Mech., Published online: 18 September, https://doi.org/https://doi.org/10.1007/s10652-020-09767-1, 2020.

French, A.: Vibrations and Waves, M.I.T. introductory physics series, Taylor & Francis, https://books.google.hu/books?id=RqE26vDmd5wC, 1971.

Garrett, C.: Internal tides and ocean mixing, Science, 301, 1858–1859, https://doi.org/https://doi.org/10.1126/science.1090002, 2003.

Inall, M., Cottier, F., Griffiths, C., and Rippeth, T.: Sill dynamics and energy transformation in a jet fjord, Ocean Dyn., 54, 307–314, https://doi.org/https://doi.org/10.1007/s10236-003-0059-2, 2004.

Johnsson, M., Green, J. A. M., and Stigebrandt, A.: Baroclinic wave drag from two closely spaced sills in a narrow fjord as inferred from basin water mixing, J. Geophys. Res.: Oceans, 112, https://doi.org/https://doi.org/10.1029/2006JC003694, 2007.

Lelong, M.-P. and Kunze, E.: Can barotropic tide — eddy interactions excite internal waves?, J. Fluid Mech., 721, 1—-27, https://doi.org/https://doi.org/10.1017/jfm.2013.1, 2013.

Massel, S. R.: Internal gravity waves in the shallow seas, Springer, 2015.

Morozov, E. G.: Oceanic Internal Tides: Observations, Analysis and Modeling: A Global View, Springer International Publishing, Cham, https://doi.org/https://doi.org/10.1007/978-3-319-73159-9, 2018.

Münnich, M.: The influence of bottom topography on internal seiches in stratified media, Dyn. Atmos. Oceans, 23, 257–266, https://doi.org/https://doi.org/10.1016/0377-0265(95)00439-4, 1996.

Niiler, P. P.: On the internal tidal motions in the Florida Straits, Deep Sea Res. Oceanogr. Abst., 15, 113–123, https://doi.org/https://doi.org/10.1016/0011-7471(68)90031-4, 1968.

Park, J., MacMahan, J., Sweet, W. V., and Kotun, K.: Continuous seiche in bays and harbors, Ocean Sci., 12, 355–368, https://doi.org/https://doi.org/10.5194/os-12-355-2016, https://os.copernicus.org/articles/12/355/2016/, 2016.

https://doi.org/10.5194/os-2020-114
Preprint. Discussion started: 16 December 2020

Parsmar, R. and Stigebrandt, A.: Observed damping of barotropic seiches through baroclinic wave drag in the Gullmar Fjord, J. Phys. Oceanogr., 27, 849–857, https://doi.org/https://doi.org/10.1175/1520-0485(1997)027<0849:ODOBST>2.0.CO;2, 1997.

Rattray Jr., M.: On the coastal generation of internal tides, Tellus, 12, 54–62, https://doi.org/https://doi.org/10.1111/j.2153-3490.1960.tb01283.x, 1960.

Rippeth, T. and Green, J. A. M.: Tides, the Moon and the kaleidoscope of ocean mixing, in: Oceanography and Marine Biology - An Annual Review, Vol. 58, edited by Hawkins, S., Allcock, A., Bates, A., Evans, A., Firth, L., McQuaid, C., Russell, B., Smith, I., Swearer, S., and Todd, P., pp. 319–350, CRC Press, https://books.google.hu/books?id=Mp4FEAAAQBAJ, 2020.

Roget, E., Khimchenko, E., Forcat, F., and Zavialov, P.: The internal seiche field in the changing South Aral Sea (2006–2013), Hydrol. Earth Syst. Sci., 21, 1093–1105, https://doi.org/https://hess.copernicus.org/articles/21/1093/2017/, 2017.

Staalstrøm, A. and Røed, L. P.: Vertical mixing and internal wave energy fluxes in a sill fjord, J. Marine Syst., 159, 15–32, https://doi.org/https://doi.org/10.1016/j.jmarsys.2016.02.005, 2016.

Stanev, E. V. and Ricker, M.: Interactions between barotropic tides and mesoscale processes in deep ocean and shelf regions, Ocean Dyn., 70, 713–728, https://doi.org/https://doi.org/10.1007/s10236-020-01348-6, 2020.

Stigebrandt, A.: Barotropic and baroclinic response of a semi-enclosed basin to barotropic forcing from the sea., in: Fjord Oceanography. NATO Conference Series (IV Marine Sciences), vol 4., edited by Freeland, H., Farmer, D., and Levings, C., pp. 141–164, Springer, Boston, MA., https://doi.org/https://doi.org/10.1007/978-1-4613-3105-6_5, 1980.

Stigebrandt, A.: Resistance to barotropic tidal flow in straits by baroclinic wave drag, J. Phys. Oceanogr., 29, 191–197, https://doi.org/https://doi.org/10.1175/1520-0485(1999)029<0191:RTBTFI>2.0.CO;2, 1999.

Stigebrandt, A. and Aure, J.: Vertical mixing in basin waters of fjords, J. Phys. Oceanogr., 19, 917–926, https://doi.org/https://doi.org/10.1175/1520-0485(1989)019<0917:VMIBWO>2.0.CO;2, 1989.

Vic, C., Naveira Garabato, A. C., Green, J. A. M., Waterhouse, A. F., Zhao, Z., Melet, A., de Lavergne, C., Buijsman, M. C., and Stephenson, G. R.: Deep-ocean mixing driven by small-scale internal tides, Nat. Commun., 10, 2099, https://doi.org/https://doi.org/10.1038/s41467-019-10149-5, 2019.

Wunsch, C. and Ferrari, R.: Vertical mixing, energy, and the general circulation of the oceans, Annu. Rev. Fluid Mech., 36, 281–314, https://doi.org/https://doi.org/10.1146/annurev.fluid.36.050802.122121, 2004.

Wynne, Z., Reynolds, T., Bouffard, D., Schladow, G., and Wain, D.: A novel technique for experimental modal analysis of barotropic seiches for assessing lake energetics, Environ. Fluid Mech., 19, 1527–1556, https://doi.org/https://doi.org/10.1007/s10652-019-09677-x, 2019.

Xue, M.-A., Kargbo, O., and Zheng, J.: Seiche oscillations of layered fluids in a closed rectangular tank with wave damping mechanism, Ocean Eng., 196, 106 842, https://doi.org/https://doi.org/10.1016/j.oceaneng.2019.106842, 2020.